View metadata, citation and similar papers at core.ac.uk
brought to you by CORE
provided by University of Southern Queensland ePrints

RESEARCH PAPER

Flexural behaviour of concrete slabs reinforced with GFRP bars and hollow composite reinforcing systems

(Title contains 14 words)

Running headline: Flexural behaviour of concrete slabs reinforced with GFRP bars and hollow composite reinforcing systems
(90 characters)

by

Mohammed Al-Rubaye[1], Allan Manalo[2], Omar Alajarmeh[3], Wahid Ferdous[4*], Weena Lokuge[5], Brahim Benmokrane[6], and Azam Edoo[7]

[1]Postgraduate student, Centre for Future Materials (CFM) , School of Civil Engineering and Surveying, University of Southern Queensland , QLD 4350, Australia. Email: mohamed.bakir3@yahoo.com,

[2]Professor, Centre for Future Materials (CFM), School of Civil Engineering and Surveying, University of Southern Queensland, QLD 4350, Australia. Email: Allan.Manalo@usq.edu.au

[3]PhD Student, Centre for Future Materials (CFM), School of Civil Engineering and Surveying, University of Southern Queensland, QLD 4350, Australia. Email: Omar.Alajarmeh@usq.edu.au

[4](*Corresponding Author) Research Fellow, Centre for Future Materials (CFM), University of Southern Queensland, QLD 4350, Australia. Email: Wahid.Ferdous@usq.edu.au

[5]Senior Lecturer in Civil Engineering, Centre for Future Materials (CFM), School of Civil Engineering and Surveying, University of Southern Queensland, QLD 4350, Australia. Email: Weena.Lokuge@usq.edu.au

[6]Professor of Civil Engineering, University of Sherbrooke, Department of Civil Engineering, Sherbrooke, Quebec, Canada. Email: Brahim.Benmokrane@USherbrooke.ca

[7]Manager, Composite Reinforcing Solutions Pty. Ltd., 48 Lucraft Gardens, Winthrop, WA 6150, Australia. Email: azam@crsperth.com

Submitted to
Composite Structures

*Corresponding Author:

Wahid Ferdous

Research Fellow,
University of Southern Queensland, Centre for Future Materials (CFM),
Toowoomba, QLD 4350, Australia
Tel: +61 7 4631 1331; Email: Wahid.Ferdous@usq.edu.au

Manuscript summary:

Total pages	32 (including 1-page cover)
Number of figures	11
Number of tables	5

Flexural behaviour of concrete slabs reinforced with GFRP bars and hollow composite reinforcing systems

Mohammed Al-Rubaye[1], Allan Manalo[2], Omar Alajarmeh[3], Wahid Ferdous[4*], Weena Lokuge[5], Brahim Benmokrane[6], and Azam Edoo[7]

[1]Postgraduate student, Centre for Future Materials (CFM) , School of Civil Engineering and Surveying, University of Southern Queensland , QLD 4350, Australia. Email: mohamed.bakir3@yahoo.com,

[2]Professor, Centre for Future Materials (CFM), School of Civil Engineering and Surveying, University of Southern Queensland, QLD 4350, Australia. Email: Allan.Manalo@usq.edu.au

[3]PhD Student, Centre for Future Materials (CFM), School of Civil Engineering and Surveying, University of Southern Queensland, QLD 4350, Australia. Email: Omar.Alajarmeh@usq.edu.au

[4](*Corresponding Author) Research Fellow, Centre for Future Materials (CFM), School of Civil Engineering and Surveying, University of Southern Queensland, QLD 4350, Australia. Email: Wahid.Ferdous@usq.edu.au

[5]Senior Lecturer in Civil Engineering, Centre for Future Materials (CFM), School of Civil Engineering and Surveying, University of Southern Queensland, QLD 4350, Australia. Email: Weena.Lokuge@usq.edu.au

[6]Professor of Civil Engineering, University of Sherbrooke, Department of Civil Engineering, Sherbrooke, Quebec, Canada. Email: Brahim.Benmokrane@USherbrooke.ca

[7]Manager, Composite Reinforcing Solutions Pty. Ltd., 48 Lucraft Gardens, Winthrop, WA 6150, Australia. Email: azam@crsperth.com

Abstract

Glass Fibre Reinforced Polymer (GFRP) bars are now attracting attention as an alternative reinforcement in concrete slabs because of their high resistance to corrosion that is a major problem for steel bars. Recently, hollow concrete slab systems are being used to reduce the amount of concrete in the slab and to minimise the self-weight, but the internal holes makes them prone to shear failure and collapse. A hollow composite reinforcing system (CRS) with four flanges to improve the bond with concrete has recently been developed to stabilise the

holes in concrete members. This study investigated the flexural behaviour of concrete slabs reinforced with GFRP bars and CRS. Four full-scale concrete slabs (solid slab reinforced with GFRP bars; hollow slab reinforced with GFRP bars; slab reinforced with GFRP bars and CRS; and slab reinforced with steel bars and CRS) were prepared and tested under four-point static bending to understand how this new construction system would perform. CRS is found to enhance the structural performance of hollow concrete slabs because it is more compatible with GFRP bars than steel bars due to their similar modulus of elasticity. A simplified Fibre Model Analysis (FMA) reliably predicted the capacity of hollow concrete slabs.

Keywords: Flexural behaviour; hollow core concrete slabs; composite reinforcing system; GFRP bars; Modelling.

1. Introduction

Reinforced concrete slabs are important structural members in building structures as they carry loads and transfer them to the beams [1, 2]. Traditionally, steel bars used as internal reinforcement inevitably corrode, which then affects the integrity of concrete slabs by reducing their strength and limiting their serviceability. The corrosion of steel bars is practically critical in structures built close to marine or industrial environments [3]. For example, the million dollar 20-storey Iluka high-rise apartment complex in Surfers Paradise, Australia which was built in 1972 was demolished in 2013 due to corrosion of the steel reinforcement in the concrete slabs and other structural elements [4]. Moreover, the Australian Corrosion Association (ACA) has reported that more than AU$10 billion is lost every year due to the corrosion of steel reinforcement [5]. Therefore, an alternative reinforcing material that will minimise or eliminate corrosion in concrete structures is deemed necessary.

Fibre reinforced polymer composites have emerged as a comparatively new construction material that can address many of the weaknesses of traditional construction materials [6]. The non-corrosive Glass Fibre Reinforced Polymer (GFRP) bars are an effective alternative reinforcing solution for concrete structures that has lower maintenance and repair costs [7]. This alternative reinforcement is lighter, non-magnetic and has higher tensile strength than steel [8, 9]. Many studies reported that GFRP bars have been used successfully as internal reinforcement for concrete structures, including beams [10], columns [11], and slabs [12]. Since slabs are the main structural members in a building that consume the largest amount of concrete and contributes significantly to the dead load [13], it should be designed to minimise the amount of materials and to reduce the overall weight. Previous researchers [14, 15] have created holes inside the slab to reduce the amount of concrete and its overall weight.

A hollow core slab (HCS) is a common structural form used for precast concrete slabs and wall panels in industrial, commercial and residential applications [16-18]. However, several researchers found that voids can cause early shear failure and significantly reduce the capacity of the slab [19, 20]. Meng [21] suggested that CFRP sheets bonded with epoxy resin and attached inside the voids would increase the shear capacity of HCS. However, this technique is not cost effective and difficult to implement, especially for small diameter voids. Cuenca and Serna [22] studied the HCS with and without fibres and they concluded that the shear capacity and ductility can be improved using fiber reinforcements. There is a need therefore to determine an efficient technology to improve structural performance of lightweight hollow core slabs. An FRP system that will create a hollow inside the slab and stabilise the voids, while fully interacting with the concrete needs to be developed.

A new type of hollow composite reinforcing system (CRS) has recently been designed and developed to create voids in reinforced concrete slabs. This CRS system has four flanges that act as shear connectors, similar to the rib shear connector in the FRP decks introduced by

many researchers to provide a composite action with concrete [23, 24]. This paper investigated for the first time the flexural behaviour of a one-way concrete slab reinforced with GFRP bars and CRS. Four concrete slabs (a solid slab reinforced with GFRP, a hollow slab reinforced with GFRP, a GFRP-reinforced slab with CRS, and a steel-reinforced slab with CRS) were cast and tested under static four-point bending to evaluate the effectiveness of the hollow CRS inside the HCS. The capacity of the hollow concrete slab was also predicted theoretically using fibre model analysis and compared with the experimental results. The results obtained from this study will aim at advancing the understanding on the behaviour of hollow concrete slabs reinforced with GFRP bars and hollow composite systems, and providing new lightweight slabs for civil engineering constructions.

2. Experimental Program

2.1. Materials

2.1.1. Hollow composite reinforcing system (CRS)

The hollow composite reinforcing system (CRS), as shown in Figure 1, was supplied by Composite Reinforcement Solutions in Australia. This material was manufactured through the pultrusion process and composed of glass fibre reinforcements (mostly unidirectional) embedded with vinylester resin. It also contains additives such as pigments, UV inhibitors, and fire retardant. The physical and mechanical properties of the CRS were evaluated in accordance with relevant ISO and ASTM standards listed in Table 1.

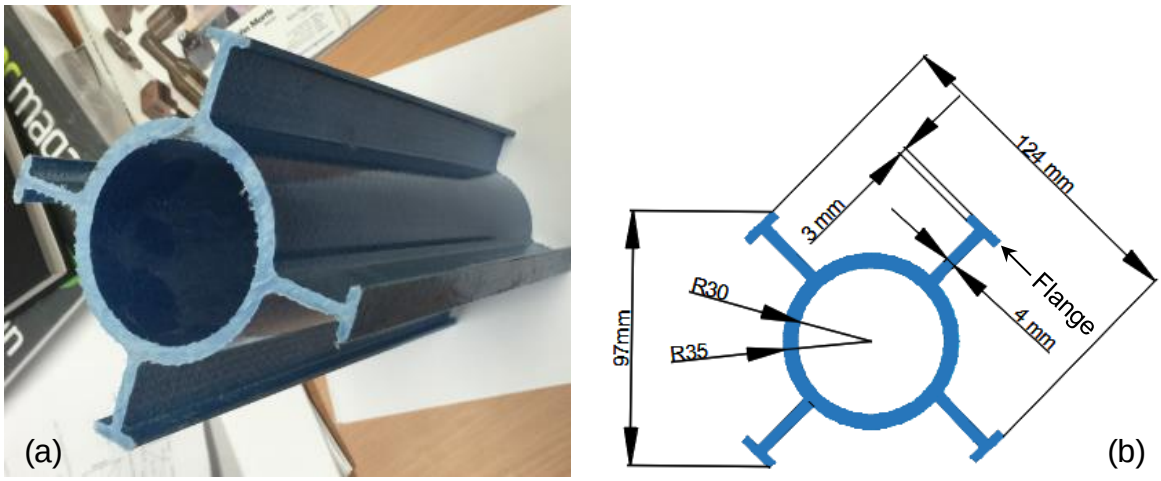

158

159 Figure 1: Details of the composite reinforcing systems (CRS) (a) shape, and (b) dimensions

160 Table 1. Physical and mechanical properties of CRS including standard deviation (SD).

Properties	Test standard	Values	SD
Density, kg/m^3	ASTM D792 [25]	1926	23.4
Fibre content by weight, %	ASTM D2584 [26]	73	2.5
Glass transition temperature, ^{o}C	ASTM E1356 [27]	81	4.2
Axial compression, MPa	ASTM D695 [28]	120	7.1
Transverse compression, MPa	ISO 14125 [29]	8.8	1.1
Transverse shear strength, MPa	ASTM D2344 [30]	7.5	0.7
Inter-laminar shear strength, MPa	ASTM D4475 [31]	22	1.5
Flexural strength, MPa	ASTM D790 [32]	201	28.7
Flexural modulus, GPa	ASTM D790 [32]	42	1.3

161

162 *2.1.2. GFRP bars*

163 The concrete slabs were reinforced with 12 mm diameter high-modulus (Grade III) GFRP bars

164 [33]. These bars were fabricated through the pultrusion process by impregnating E-type glass

165 fibres in a thermosetting modified vinyl-ester resin. The external surfaces of the GFRP bars

were coated with particles of silica-sand to enhance the bond between the reinforcement and surrounding concrete. The mechanical properties of these bars are reported by Benmokrane et al. [34] and summarised in Table 2.

Table 2. Mechanical properties of GFRP bars [34].

Properties	Test standard	Values	SD
Flexural strength, MPa	ASTM D4476 [35]	1588	93
Interlaminar shear strength, MPa	ASTM D4475 [31]	53	2.1
Longitudinal tensile strength, MPa	ASTM D7205 [36]	1281	35
Longitudinal tensile modulus, GPa	ACI 440.6M [37] and CSA S807 [33]	61	0.4
Longitudinal tensile strain at failure, %	ACI 440.6M [37] and CSA S807 [33]	2.1	0.1

2.1.3. Steel bars

The steel reinforcing bars were standard grade 500N with a nominal diameter of 12 mm. The characteristic strength and Young's modulus of the reinforcing steel as supplied by the manufacturer were 500 MPa and 200 GPa, respectively.

2.1.4. Concrete

The ready mix concrete with a nominal compressive strength of 32 MPa was used. The maximum size of aggregate was 10 mm and the slump value of the concrete was 100 mm in accordance with AS1379 specification [38]. A total of 8 cylinders were prepared and tested as per AS1012 standards [39] at the time of testing the slabs. The average compressive strength of concrete was 31.8 MPa with a standard deviation of 3.54 MPa while the modulus of elasticity was measured as 29.9 GPa.

2.2. Slab details

Four full-scale slabs, 2400 mm long by 750 mm wide by 175 mm thick were prepared. These dimensions are based on industry practice for precast hollow core slabs. Of these four slabs, one solid slab reinforced with GFRP bars (S1), one hollow slab reinforced with GFRP bars (S2), one GFRP reinforced slab with CRS (S3), and one slab was reinforced with steel bars and CRS (S4). Slabs S1, S2, and S3 were reinforced with 12 mm diameter GFRP bars spaced 200 mm (both longitudinally and transversely) at the top and bottom, while slab S4 was reinforced with 12 mm diameter steel bars instead of GFRP but maintained the same reinforcement arrangement for comparison. The reinforcement ratio was ρ = 0.44% for all slabs that resulted in an over-reinforced section for slabs S1 to S3 (balanced reinforcement ratio, ρ_b = 0.25%) and an under-reinforced section for slab S4 (ρ_b = 2.1%) as per the CSA S806 [40]. Reinforcement ratio of 0.44% for GFRP-reinforced slabs was adopted from the specification provided in ACI-15 code by having at least 1.4 as a ratio between the actual reinforcement-to-balanced conditions. The reinforcement ratio was adopted to achieve a flexural compression failure in concrete and provide high deformation capacity and less brittle failure rather than tensile rupture of the GFRP bars. Slab S2 was fabricated with three holes, 70 mm diameter in each and spaced at 300 mm while slabs S3 and S4 were manufactured with three hollow CRS of equal diameter and spacing. A 15 mm thick cover of concrete was provided at the top and bottom reinforcements, and a 25 mm thick cover of concrete was provided at the edges of the slabs. The geometric dimensions and reinforcement arrangements are provided in Table 3. It is noteworthy that one CRS has a cross-sectional area of 1585 mm^2, which is 1.63% of the gross sectional area of the slab. Therefore, the three CRS is 4.89% of the total gross sectional area of the concrete. However, the main function of the CRS is to stabilise the holes while the longitudinal GFRP bars provide the longitudinal reinforcement to carry flexural loads.

Table 3. Concrete slab details

Slab	Cross section layout	Description
S1	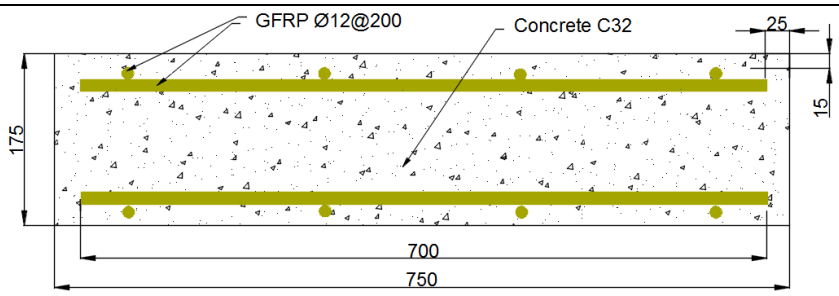	Solid concrete slab reinforced with GFRP bars
S2	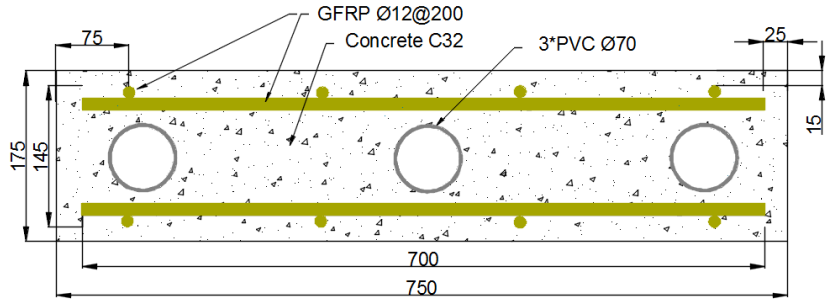	Hollow concrete slabs reinforced with GFRP bars
S3	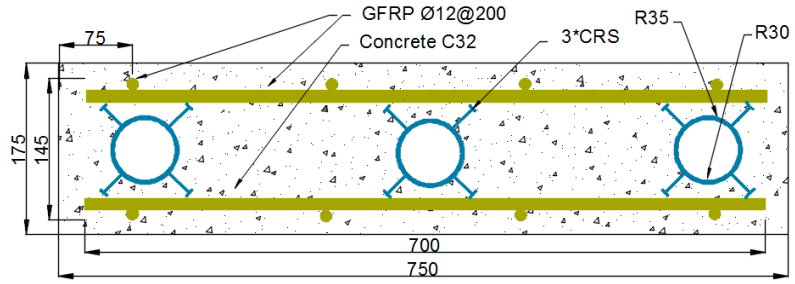	Slab reinforced with CRS and GFRP bars
S4	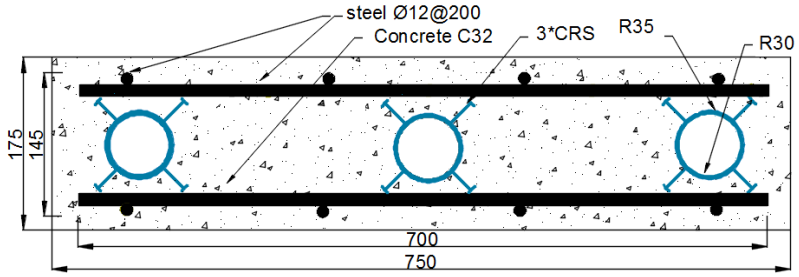	Slab reinforced with CRS and steel bars

2.3. Specimen preparation

All the reinforcements were assembled on a work table with patterns drawn to ensure the bars were spaced properly, and cut sections of CRS were used as spacers between the top and bottom reinforcement for slabs S1 and S2. Moreover, PVC pipes (70 mm outside diameter by 1mm

thick wall) were used to create holes inside the concrete in slab S2 as shown in Figure 2(a). For slabs S3 and S4, the CRS were spaced equally at 300 mm centres and tied up to the top and bottom longitudinal reinforcements to prevent movement while casting concrete. Uni-axial strain gages with a gauge length of 3 mm were attached at the top and bottom reinforcements at mid-span and at the top surface of the CRS to measure strain during loading, as shown in Figure 2(b). Moreover, 20 mm uni-axial strain gauges were attached at the top and bottom concrete surfaces of the slabs. Bent 12 mm diameter steel bars were placed at each corner of the slabs as lifting hooks to facilitate handing and setting during test.

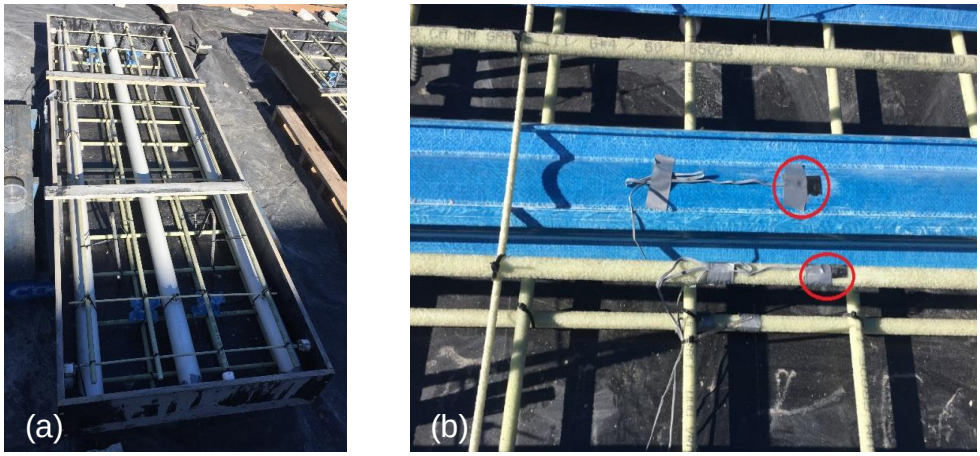

Figure 2: Assembly of reinforcement and attachment of strain gauges (a) slab S2 with PVC pipes before casting and (b) strain gauges attached to the bars and CRS

2.4. Test set-up and instrumentation

The slabs were tested under four-point static bending with a shear span-to-depth ratio of 5.1, as shown in Figure 3. The load was applied through a spreader steel I-beam using a 2000 kN Enerpac hydraulic rams, and measured using a 444 kN load cell. All the specimens were tested under displacement control mode at a rate of 5 mm/min. Rubber matting was placed under the loading steel plate to ensure a uniform load distribution to the slab. A laser displacement transducer was used to measure mid-span deflection at the bottom of the slab. Prior to testing, gridlines were marked on the front side of the slab to trace the propagation of cracks during

234 loading. The applied loads, deflections and strains were recorded using Vishay System 5000.

235 All the specimens were tested up to the ultimate failure.

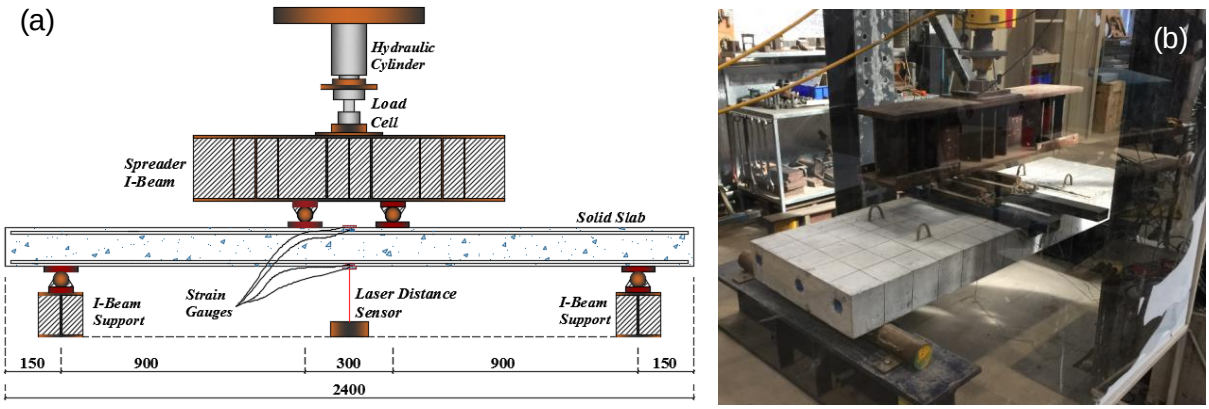

236

237 Figure 3: Test set-up and instrumentation (a) schematic diagram and (b) actual test set up

238

239 **3. Test Results and Observation**

240 ***3.1. Crack propagation and failure behaviour***

241 Table 4 reports the moment at first cracking, stiffness before cracks, maximum bending moment,

242 stiffness after cracks and the failure mode of the slabs at the ultimate load.

243 Table 4. Experimental failure modes of reinforced concrete slabs

		First crack			Maximum			
Slab	Mass	Load	Moment	Stiffness before cracks	Load	Moment	Stiffness after cracks	Failure
	Kg	kN	kN-m	kN/mm	kN	kN-m	kN/mm	
S1	772	27	12.2	6.49	137	62	2.58	Mode I
S2	713	30	13.5	5.21	145	65	2.43	Mode I
S3	718	27	12.2	6.91	211	95	4.93	Mode II
S4	731	24	10.8	8.57	208	94	7.93	Mode III

244 Mode I: Flexure-shear crack with concrete crushing under the loading point and buckling of the

245 bars

Mode II: Concrete crushing at mid span with horizontal cracks

Mode III: Steel yielding followed by concrete crushing at mid span

Figure 4 shows the propagation of cracks in the slabs where the number next to the crack indicates the corresponding applied load in kN. The first crack occurred at the bottom in between the loading points at an applied load of 27 kN, 30 kN, 27 kN and 24 kN for slabs S1, S2, S3, and S4, respectively. The propagation of cracks in slabs S1 and S2 were similar with the increase of loads, as shown in Figures 4(a) and 4(b). Fine vertical cracks began at the bottom of the slab near the loading points up to a load of 70 kN, and then the vertical cracks widened and propagated towards the top of the slab. At a load of 140 kN, the concrete began to be crushed on the compression side under the loading point. As the load continued, the flexural vertical cracks inclined under the shear effect towards the top under the loading point. This was followed by the concrete compression crushing and the compression buckling of top GFRP bars that caused slabs S1 and S2 to fail completely. More severe concrete crushing through the depth was observed in slab S2 when comparing with S1, as shown in Figures 5(a) and 5(b). This indicates the holes in slab S2 collapsed at the time of ultimate failure. No noticeable changes were observed in the bottom GFRP reinforcements for slabs S1 and S2.

Similar crack propagation occurred in slabs S3 and S4 up to an applied load of 140 kN, as shown in Figures 4(c) and 4(d), after that the cracks in slab S4 became wider than in slab S3 due to the yielding of steel. With further increase of load, horizontal cracks were developed in slab S3 started under the loading points and propagated along the length of the CRS (Figure 5c). The final failure occurred due to the concrete crushing at the midspan of slabs S3 and S4 (Figures 5c and 5d). A loud noise was also heard due to the damage of fibres in the bottom flanges of the CRS as the top and bottom reinforcements did not rupture.

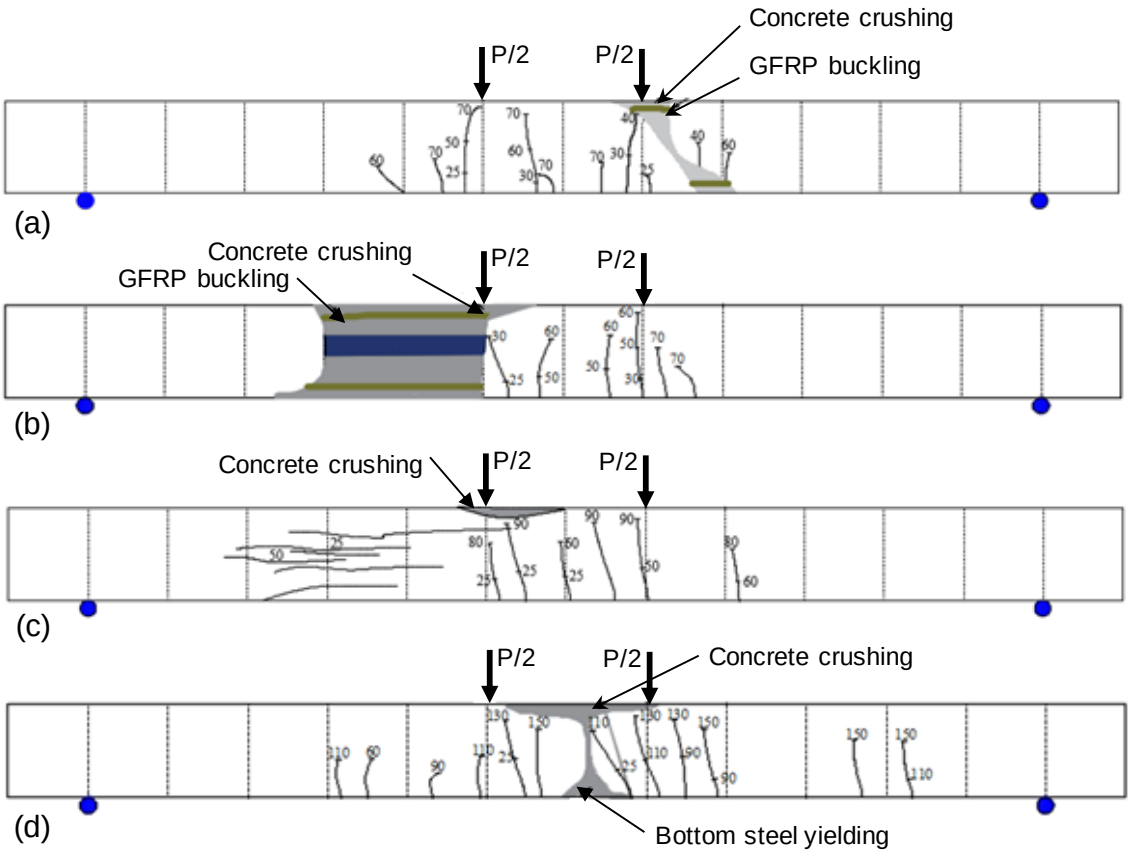

Figure 4: Crack propagation (a) slab S1, (b) slab S2, (c) slab S3, and (d) slab S4

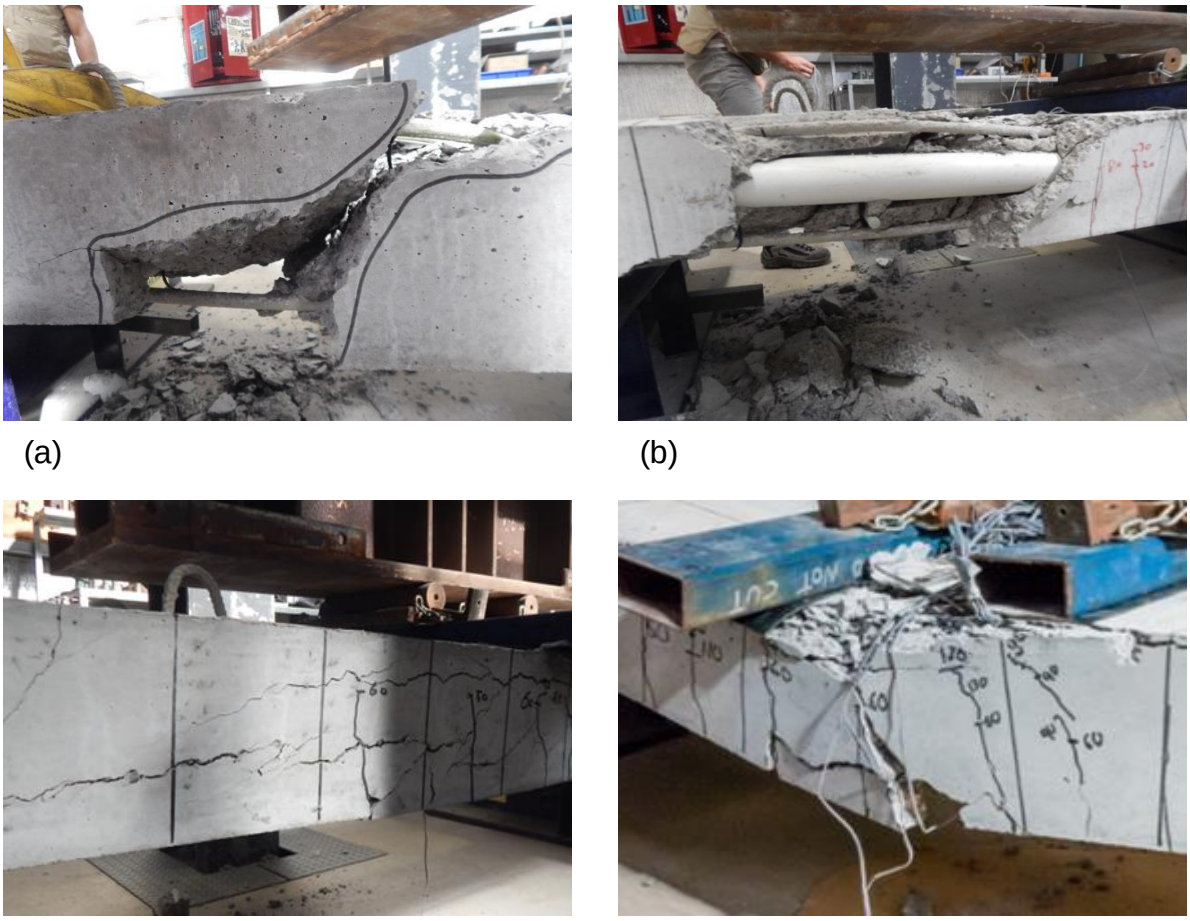

Figure 5: Final failure (a) slab S1, (b) slab S2, (c) slab S3, and (d) slab S4

3.2 Load-deflection behaviour

Figure 6 shows the load-mid span deflection of the four tested slabs. The initial settlement effect at the beginning caused by rubber mat was carefully eliminated when plotting load-displacement curve. Every slab exhibited linear load-deflection until the concrete experienced its first flexural cracking at 25 kN and a deflection of 3 mm. When the concrete cracked, slabs S1 and S2 experienced a significantly reduced stiffness (60% drop for S1 and 53% drop for S2) but maintained the similar trend. The deflection increased linearly with the increase of loads up to around 140 kN and a deflection of 50 mm. Thereafter, both slabs experienced a nonlinear behaviour as the concrete began to crush and develop flexure-shear cracking at the loading point

(Figures 4a and 4b). Both slabs then failed abruptly with a midspan deflection of around 60 mm due to flexure-shear failure, as shown in Figures 5(a) and 5(b).

The slope of the load-deflection curve in slab S3 decreased from 6.91 kN/mm to 4.93 kN/mm (29% drop) after the first crack of concrete. At this stage, the deflection increased linearly up to around 200 kN load and a deflection of 46 mm. After that the load increased non-linearly and reached up to 211 kN with a deflection of 57 mm. The load cpacity then began to decrease until the failure at a deflection of 80 mm. Unlike S3, slab S4 showed lower stiffness drop (7%) after cracking the bottom concrete. Deflection then increased linearly with load up to around 130 kN. The slope of the load-deflection curve decreased again after this load, and the behaviour of slab S4 became nonlinear until it reached to a maximum load of 208 kN with a deflection of 45 mm. There was a slight decrease in the load capacity after the peak and the slab continued to deflect even without any increase in the load. The ultimate failure of the slab S4 occurred at a midspan deflection of 76 mm due to the concrete crushing and steel buckling, as shown in Figure 5(d).

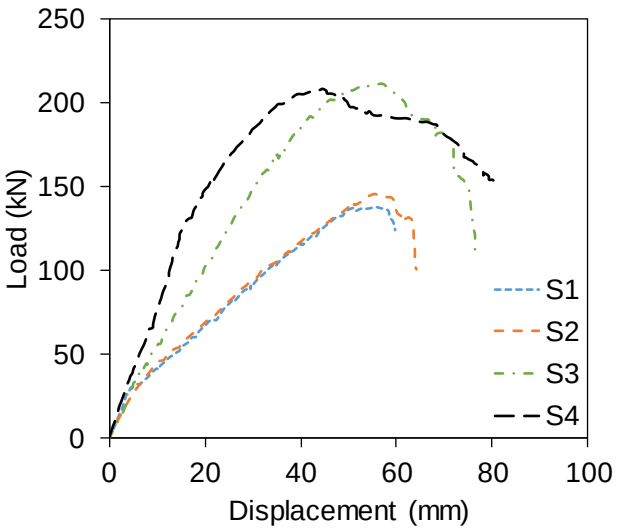

Figure 6: The load-deflection relationship of concrete slabs

To verify the reliability of the experimental results, a nonlinear finite element (FE) analysis for slab S3 has been conducted using ANSYS Mechanical APDL [41]. Solid 65 three-dimensional element was used to model concrete that has the capability of capturing nonlinear material properties, plastic deformation, crushing in compression and cracking in tension. The CRS profiles were modelled with a Shell 181 element that is suitable for analysing thin to moderately-thick structural component. A Beam 188 element was used to model FRP bars that is suitable for analysing slender to moderately thick beam structures while the loading and support plates were modelled with a Solid 186 element. Mapped meshing with a maximum element size of 10 mm and approximate aspect ratio of one were used for half slab. The symmetric plane were subjected to symmetric boundary conditions. The concrete crushing and cracking stresses of 32 MPa and 2.26 MPa, respectively, and open and closed shear transferred coefficients of 0.2 and 0.8, respectively were used in the model. Orthotropic properties of CRS fibre composite profiles and isotropic properties of FRP bars as provided in Table 1 and Table 2 were used. Loads were applied at top nodes of the loading plate while the supports were restrained in X and Y directions to simulate the experimental testing conditions. Figure 7(a) shows that the cracking of bottom concrete started at around 24 kN which is to similar the experimental crack observation at 25 kN. The increase of load gradually increase the propagation of cracks. The deflection behaviour of the slab at peak load (220 kN) is shown in Figure 7(b) where it can be seen that the maximum deflection is approximately 40 mm that is close to the experimental deflection at peak load for S3 specimen. This FE result confirmed that the experimental data are reliable and valid.

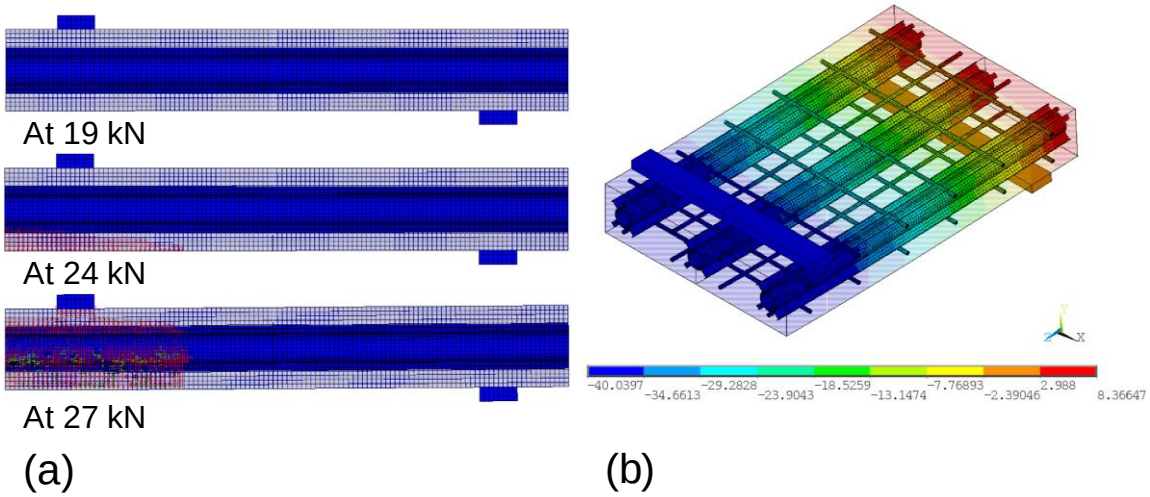

Figure 7: FE analysis (a) concrete cracking and crushing plot and (b) deflection at peak load of S3 specimen

3.3 Load-strain behaviour

Figure 8 shows the load-strain relationship for top concrete, bottom bars, top bars, and top of CRS of all four slabs. Figure 8(a) shows that the strain of the top concrete increased linearly up to 100 microstrains until occuring the first flexural tensile cracks at the bottom of the slabs at a load of approximately 25 kN. The strain then increased linearly but at a faster rate than before cracking and continued until the failure of slabs S1, S2 and S3. The maximum strain recorded in the top concrete was 2100 microstrains, 1995 microstrains, and 2855 microstrains for slabs S1, S2, and S3, respectively. The lower strain in top concrete in slabs S1 and S2 further confirmed the observed flexure-shear failure while slab S3 failed in bending. After the bottom concrete began to crack, strain at the top of the concrete for slab S4 also increased linearly but at a slower rate than the other three slabs. However, the strain increased nonlinearly at a load of 130 kN and strain of 1100 microstrains. It is noted that the top concrete strain gauge stopped recording data just after the peak load (202 kN) at 1791 microstrains due to the initiation of concrete crushing caused by steel yielding.

Figure 8(b) shows the load-strain relationship of bottom bars for all slabs. There was no noticeable changes of strain in the bottom GFRP bars before the concrete tensile cracking at around 25 kN load while the strain increased rapidly thereafter. The load-strain behaviour in the tensile GFRP bars for slabs S1 and S2 was found similar, and the strain reached to 13,000 microstrains at failure. The load-strain behaviour in slab S3 was almost linear after the first flexural tensile crack of the concrete, however, the rate of increase of strain was slower than slabs S1 and S2. The nonlinearity started when the load reached to the peak at around 211 kN. The strain measured at the bottom of GFRP bars when slab S3 finally failed was around 14,000 microstrains, which was almost 70% of the failure strain of the GFRP bars in tension. As expected, the strain in the bottom steel bars for slab S4 developed at a slower rate than the GFRP bars in slabs S1 to S3. However, the strain remained constant at around 2700 microstrains from 130 kN to 208 kN, which is the level of yield strain for 500 MPa steel bars. This was followed by a large increase in strain even without any further increase in the applied load.

Figure 8(c) shows the relationship between load and strain of the compression reinforcement for slabs S3 and S4. The graph shows that the strain in the compressive GFRP bars in slab S3 increased linearly with load even after the bottom concrete began to crack. However, the load-strain behaviour became nonlinear near to the peak at 170 kN. The maximum strain recorded was around 2400 microstrains. On the other hand, the load-strain behaviour in the top steel bars for slab S4 was nonlinear from concrete cracking to the failure. Over 3000 microstrains were recorded in the steel bars in compression at failure. Figure 8(d) shows the load-strain relationship at the top surface of the CRS for slab S3 and S4. Both slabs showed very small strain at the top of the CRS up to 150 kN. After that the strain increased nonlinearly until the slab reached to the peak load and observed that the strain in slab S3 was slightly higher than slab S4 at the same level of load. The CRS in slab S4 reached almost 7100 microstrains before it failed whereas the maximum strain recorded in slab S3 was only 2500 microstrains.

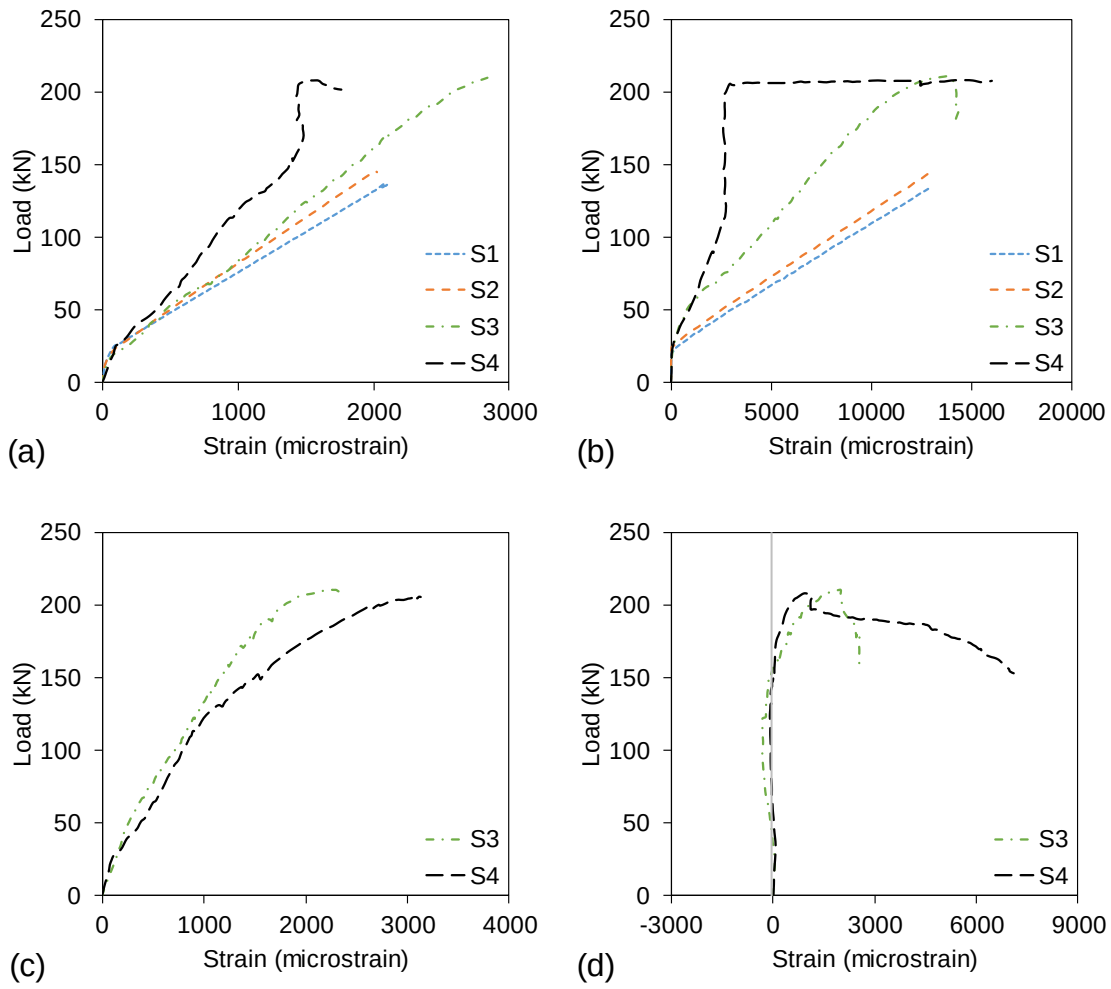

Figure 8: Load-strain behaviour for (a) top concrete, (b) bottom bars (GFRP and steel), (c) top bars (GFRP or steel), and (d) top of CRS

4. Discussion

4.1. Influence of the hollow core

The influence of a hollow core in a precast concrete slab reinforced with GFRP bars was evaluated by comparing the behaviour of slabs S1 and S2. Results indicated that the structural behaviour of solid and hollow core slabs was similar as both slabs exhibited same cracking propagation and failed by the concrete crushing and buckling of bars under compression

followed by a diagonal crack. The diagonal crack observed in slabs S1 and S2 is due to the flexure and shear effect as the crack started from the bottom and propagated diagonally towards the top. This can be further confirmed by shear resistance capacity of the slab estimated using Canadian code [40], Australian code [42], American code [43] and Italian code [44] as expressed in Eq. (1), Eq. (2), Eq. (3) and Eq. (4), respectively. The estimated shear resistance of the solid slab (S1) is 84 kN, 80 kN, 100 kN, and 93 kN, while for the hollow slab (S2) is 62kN, 61 kN, 74 kN, and 68 kN based on CSA-S806 [40], AS-3600 [42], ACI-318 [45], and CNR-DT 203 [44] standards, respectively. These results are close to the experimental shear force (half the applied load) developed at failure of slab S1 (68.5 kN) and S2 (72.5 kN). This finding refers to the shear effect in the final failure of S1 and S2. However, the failure of hollow core slab (S2) was more brittle than the solid slab (S1) due to the catastrophic collapse of the holes. Cuenca and Serna [22] stated that this type of failure is expected for hollow core concrete slab because of the reduced width of the web that cannot resist the shear forces.

According to CSA-S806 standard [40],

$$V_c = 0.05\lambda\phi_c k_m k_r (f_c')^{1/3} b_v d_o \qquad (1)$$

where, $0.11\phi_c (f_c')^{1/2} b_v d_o \leq V_c \leq 0.22\phi_c (f_c')^{1/2} b_v d_o$

According to AS-3600 standard [42],

$$V_c = \beta b_v d_o f_{cv} \left(\frac{A_f}{b_v d_o}\right)^{1/3} \qquad (2)$$

According to ACI-318 code [45],

$$V_c = 2\lambda\sqrt{f_c'} b_v d_o \qquad (3)$$

According to CNR-DT 203 code [44],

$$V_c = 1.3 \left(\frac{E_F}{E_S}\right)^{\frac{1}{2}} . \tau_{Rd} . k . (1.2 + 40\rho) b_v d_o \qquad (4)$$

In Eqns. (1 to 3), V_c is the total shear resistance, $\beta = 1.1(1.6 - \frac{d_o}{1000})$, $\lambda = 1$, and $\phi_c = 0.6$ are factors to account for concrete, $k_m = \sqrt{\frac{V_f d_o}{M_f}} \leq 1$ and $k_r = 1 + (E_F.\rho)^{1/3}$ are the moment and reinforcement coefficients ,respectively, where M_f and V_f are the factored moment and shear forces, respectively, E_F, E_S and ρ_F are the elastic modulus of the GFRP bars and steel, respectively, and the longitudinal reinforcement ratio. The $\tau_{Rd} = (0.15\sqrt{f_c'})$ and $k = 1$ are the design shear stress of the concrete and reinforcement coefficient, respectively. The f_c' and A_f are the concrete strength and area of reinforcement, b_v and d_o are the width of the slab and depth of reinforcement, $f_{cv} = (f_c')^{1/3} \leq 4$ MPa. It is important to note that Eq. (1), Eq. (2) and Eq. (4) are based on SI unit whereas Eq. (3) is based on FPS unit.

Creating holes in the slab that reduced the gross cross-sectional area by 9% has an effect on initial bending stiffness, however, it did not affect significantly on the capacity. The stiffness of the slabs S1 and S2 were measured at 6.49 kN/mm and 5.21 kN/mm while the capacity obtained were 137 kN and 145 kN, respectively (Table 4). The lower stiffness of S2 than S1 is due to the reduced width of the slab at the initial location of neutral axis. However, the bottom concrete started cracking with the increase of loads and the neutral axis gradually shifted upwards. At a maximum load point, the similar behaviour and capacity of slabs S1 and S2 can be attributed to the location of neutral axis that is above the top of the hollow core where the uncracked concrete in compression were behaving same for both slabs. Using the strain measured at the top concrete in Figure 8(a) and bottom reinforcement in Figure 8(b), the neutral axis at the loads of 40 kN, 70 kN, 90 kN, 125 kN and 145 kN was calculated to be 18.48 mm, 14.79 mm, 14.36 mm, 13.50 mm and 13.33 mm, respectively, which clearly indicated the neutral axis was above the holes, as shown in Figure 9.

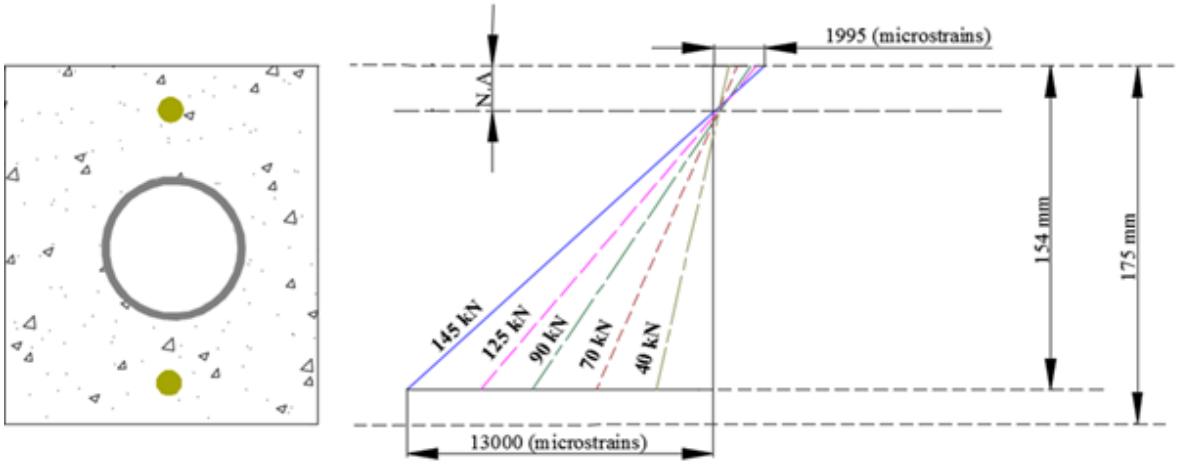

Figure 9: Strain distribution in slab S2

4.2. The effectiveness of CRS as reinforcement

The effect of CRS was investigated by studying the behaviour of slabs S2 and S3. The incorporation of three pieces of CRS in slab S3 provided 45% higher capacity than slab S2, indicating that the CRS was acting as internal flexural and shear reinforcement for slab S3. This finding can be supported by the load-strain behaviour of the bottom GFRP bars (Figure 8b) where the addition of CRS reduced the strain in the bottom bars for slab S3. CRS also increased the bending stiffness of hollow concrete slab by 33% (from 5.21 kN/mm to 6.91 kN/mm) while it reduced the loss of stiffness by 24% (53% loss for S2 and 29% loss for S3) after first crack. Due to the linear load-deformation behaviour of the GFRP-reinforced slabs, deformability factor is used as an overall performance indicator suggested by CSA S6 code [46] instead of ductility factor related to steel-reinforced slab counterparts. Deformability factor is the ratio between the maximum moment times the corresponding curvature or deflection divided by the moment value times the corresponding curvature or deflection when concrete records 1000 microstrains, where this ratio is limited to 4 as a least value. Accordingly, providing CRS in slab S3 significantly increased the deformability factor from 4.09 to 8.86 representing 117% increase compare to slab S2. Moreover, the CRS changed the failure modes from flexure-shear in S2 to almost pure flexure observed in S3. The CRS also minimised the propagation of vertical

flexural cracks and prevented the massive concrete crushing at the final failure. CRS controlled the direction of cracking and made the crack path longer because they needed to pass through the CRS flanges, thereby enhancing the serviceability performance of slab S3. The hollowness of the CRS increased significantly the stiffness and strength of the slab without increasing the weight. This improvement cannot be achieved with just conventional reinforcement or GFRP bars without the additional weight due to the increase in amount of reinforcement. The enhancement of the performance of hollow core slab using CRS was found better than the carbon fibre reinforced polymer (CFRP) sheets implemented by [21] where the load capacity only increased by 11%. This was because the latter method could not prevent the hollow core from collapsing. It is worth mentioning that no debonding failure was observed in slab S3 as because the four flanges of the CRS interacted effectively with the concrete. On the other hand, the debonding failure seen by [21] for externally bonded CFRP sheets could have been prevented by providing thicker sheets internally and that is how CRS is working. Elgabbas et al. [47] observed improvement in the load carrying capacity of the hollow core concrete slabs reinforced internally with thin CFRP sheets but shear failure still occurred due to the debonding of CFRP sheets from the concrete. More interestingly, the addition of GFRP bars with equivalent area of CRS could not achieve such enhancement in stiffness and strength without increasing the cross-sectional area of the slab due to the significant increase in the ratio between the actual reinforcement-to-balanced condition, wherein El-Nemr et al. [48] indicated that this condition will result in insufficient improvement in carrying loads. This result also indicates that a thinner concrete slab with CRS is possible to achieve the same strength and stiffness of solid and hollow slab resulting in a more lightweight and economical structure.

4.3. Effect of reinforcing materials

Finding the influence of using different reinforcing materials in concrete slabs was achieved by testing slabs S3 and S4. The types of reinforcement had a signficant effect on the overall stiffness but none on the load capacity of the hollow concrete slabs. After first crack, slab S4 retained almost 93% of its initial and uncracked stiffness while slab S3 retained 71%. Slab S4 was stiffer because the modulus of elasticity of steel used in it was higher than the GFRP bars in slab S3, as also observed by many researchers [7, 10, 49, 50]. However, the provision of CRS enabled the GFRP reinforced hollow concrete slab to retain most of its stiffness because it prevented developing wider flexural cracks. For example, El-Gamal et al. [51] found that the steel reinforced slab was almost 72% stiffer than the slabs reinforced with GFRP with a similar reinforcement ratio while in the present study the steel reinforced slab (S4) was only 33% stiffer than slab S3. Moreover, the flexural capacity of slab S3 (211 kN) and S4 (208 kN) were almost same because the failure behaviour of both slabs was governed by compressive crushing of the top concrete followed by failure of the CRS due to the combination of bending and interlaminar shear failure. Figure 8 shows that the addition of CRS reduced the amount of strain experienced by the GFRP bars (slab S3) thus indicating how well it utilises the tensile strength of the bars. Morever, the GFRP bars and CRS were recorded the highest contribution in the final load. Notwithstanding this, all of the stress was transferred to the CRS when the tensile reinforcement in slab S4 yielded at a load of 140 kN. The bottom steel reinforcement stopped recording the strains while the strain in the CRS increased markedly after the steel bars yielded up to their maximum load (Figure 8). Slab S4 then continued to carry the load until the CRS failed, and then the stiffness decreased in the load-deflection behaviour when the steel yields (Figure 6) showing almost similar stiffness to slab S3 until the maximum load capacity. This result contradicts the comparison between the stiffness as slab S4 reinforced with steel was stiffer than S3 from the time the concrete began to crack until the steel yielded. However, a different trend was observed after yielding as S3 slab showed continuous linear stiffness due to the linear

elastic behaviour of GFRP bars while in S4 the steel stopped resisting. On the other hand, it can be noticed that slab S3 shows a slightly higher area under the load-deformation curve (see Figure 6) compare to slab S4, indicating that the CRS improved the deformability of slab S3 and energy absorption. This suggests that the GFRP bars and CRS combination are more compatible than steel bars and CRS combination because the stiffness of GFRP and CRS are almost the same.

The presence of CRS prevented the premature compressive failure of concrete but still developed horizontal shear cracks at the level of the hollow reinforcing system. However, there were more and deeper horizontal cracks in slab S3 than in slab S4. Chang and Seo [52] studied GFRP-reinforced and steel-reinforced one way slabs with similar dimensions and reinforcement ratio. They observed wider cracks in GFRP-reinforced slab than in the steel-reinforced one because of the low modulus of GFRP bars. The lower stiffness of GFRP bars than steel bars also explains why the deflection in slab S3 was higher than in slab S4. At the maximum load, compressive crushing of the concrete began in slab S3 whereas the bottom steel in slab S4 yielded.

5. Theoretical evaluation of the flexural capacity of CRC slabs

5.1. Fibre model analysis

The behaviour of concrete slabs with hollow composite reinforcing system in flexure was predicted using a simple Fibre Model Analysis (FMA). This layer-by-layer approach was successfully implemented by previous researchers [53-55] in predicting the flexural capacity of composite structures. In this design approach, the capacity of hollow concrete slabs is based on the force equilibrium, strain compatibility, and constitutive behaviour of the materials. The internal force equilibrium principle was applied to determine the flexural capacity based on the properties of the constituent materials. It was assumed that a perfect bond exists between the reinforcement and concrete, and the strain in each layer was directly proportional to their

distance from the neutral axis. The sectional equilibrium was maintained by balancing the internal compressive and tensile resistance of the section, indicating varying locations of neutral axis with the increase of loads. For simplicity, the four rectangular flanges (Figure 1b) were converted to an equivalent circular area (Figure 10) for slabs with hollow composite reinforcing system. The top CRS bars were located at 42.5 mm from the top concrete layer while the bottom CRS bars were positioned at the same distance from bottom concrete layer. The unit sectional geometry, strain and stress diagrams are shown in Figure 10.

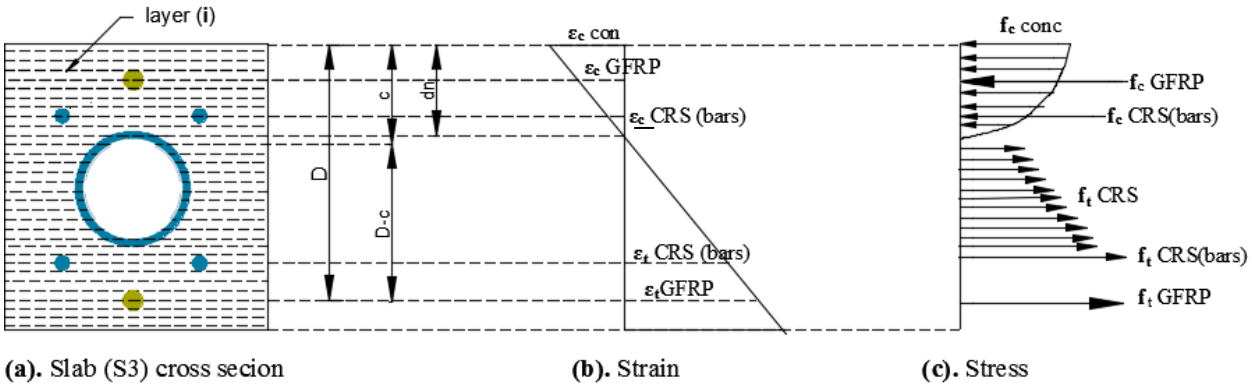

Figure 10: Basic assumptions in FMA

In Figure 10, D is the effective depth, c is the depth of any layer from the extreme compression fibre, d_n is the depth of neutral axis while $\varepsilon_{c\ con}$, $\varepsilon_{c\ GFRP}$, $\varepsilon_{t\ GFRP}$, $\varepsilon_{c\ CRS}$, and $\varepsilon_{t\ CRS}$ are the top concrete strain, top and bottom GFRP strain, and top and bottom CRS strain, respectively. On the other hand, $f_{c\ conc}$, $f_{c\ GFRP}$, $f_{c\ CRS}$ and $f_{c\ CRS\ (bars)}$ are the compressive stress of concrete, GFRP bars, CRS and CRS bars, respectively. While $f_{t\ CRS}$, $f_{t\ CRS\ (bars)}$ and $f_{t\ GFRP}$ are tensile stress of CRS, CRS bars and GFRP bars, respectively. Different assumptions have been considered in the FMA including or excluding tensile contribution of concrete and CRS flanges. The GFRP bars and CRS were analysed as linear elastic material in both tension and compression while the steel was simplified with a bilinear behaviour [56], i.e. linear elastic before yielding and a constant stress after yield. The constitutive models for concrete, CRS, GFRP bar and steel bar are shown in Figure 11.

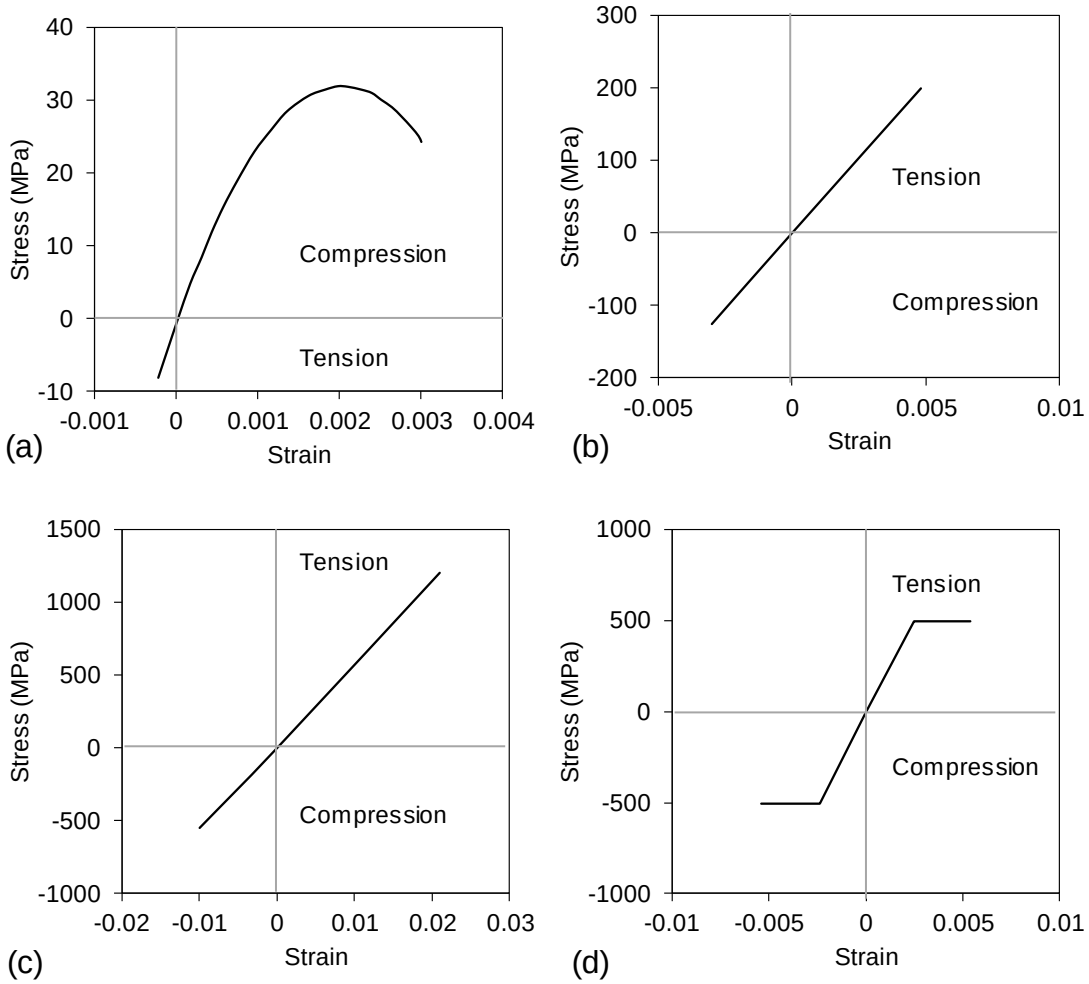

Figure 11: Constitutive materials model (a) concrete, (b) CRS, (c) GFRP bar and (d) steel bar

The concrete crushing failure criterion (assuming strain at top concrete 0.003) was considered in FMA. While the slab remains uncracked, all the layers or element *i* contribute to the moment capacity of the section. The strain at different levels were calculated using the concept of similar triangles as given in Eq. (5). The corresponding neutral axis depth (d_n) were adjusted for the strains in the top and bottom which set the force equilibrium principle calculated using Eq. 6. The stress were then determined from the constitutive material model in Figure 11 based on the strain for each layer. The moment capacities of the hollow core slabs were predicted using Eq. 7.

$$\varepsilon_i = \frac{\varepsilon_{c\,con} \times (dn - di)}{dn} \quad (5)$$

$$\sum P = \sum_{i=1}^{n} f_{i,conc}\ A_{i,conc} + \sum_{i=1}^{n} f_{i,CRS}\ A_{i,CRS} + \sum_{i=1}^{n} f_{i,GFRP}\, A_{i,GFRP} = 0 \quad (6)$$

$$\sum M = \sum_{i=1}^{n} f_{i,conc}\ A_{i,conc} di + \sum_{i=1}^{n} f_{i,CRS} A_{i,CRS}\ di + \sum_{i=1}^{n} f_{i,GFRP} A_{i,GFRP}\ di \qquad (7)$$

In Eqs. (4-6), $\mathcal{E}_{c\ con}$ and $\mathcal{E}_i$ are the top concrete strain and concrete strain at depth d_i. Moreover, P, $f_{i,conc}$, $A_{i,conc}$, $f_{i,GFRP}$, $A_{i,GFRP}$, $f_{i,CRS}$, $A_{i,CRS}$, M and d_i indicate the load capacity, concrete strength at layer i, concrete area at layer i, strength of GFRP bar, area of main reinforcement at layer i, CRS strength at layer i, CRS area at layer i, bending moment capacity, and layer depth from upper compressive layer. The total number of layers (n) is 175 layers.

5.2 Predicted failure load and comparison with the experiments

The flexural capacity is calculated for S3 and S4 slabs as they are failed in flexure while the other two slabs S1 and S2 were failed in flexure-shear, thus, FMA is not an ideal approach to estimate the failure loads for the latter case. Table 5 presents a summary of the loads predicted under different criteria and compares them with the results from the experiment. It can be seen that the closest prediction was obtained when the contribution of the tensile strength of concrete (Stiffening behaviour) and the flanges of the CRS were accounted. In general, the capacity of the slab with CRS can be predicted as close as 13.8% to the actual load measured from the experiments. The small difference between the predicted load and the actual failure load can be attributed to many reasons including the inherent variability of the compressive strength of concrete, the contribution of the flanges in keeping more concrete intact, and the partial consideration of the CRS (the small web portion perpendicular to flanges did not consider) in the FMA.

Table 5. Predicted and actual failure loads

Considerations	Capacity of S3 (kN)		Difference (%)	Capacity of S4 (kN)		Difference (%)
	FMA	Exp.		FMA	Exp.	

Ignored tensile strength of concrete and CRS flanges	156	211	26.1	146	29.8
Ignored tensile strength of concrete and accounted CRS flanges	167		20.9	166	20.2
Accounted tensile strength of concrete and ignored CRS flanges	171		19.0	157	24.5
Accounted tensile strength of concrete and CRS flanges	182		13.7	173	16.8

6. Conclusions

This study investigated the flexural behaviour of one-way concrete slabs reinforced with GFRP bars and hollow composite reinforcing systems. Full-scale concrete slabs were tested under four-point static bending to observe the propagation of failure, load-deflection, and the load-strain behaviour. The failure load of hollow concrete slabs was also predicted using the simplified Fibre Model Analysis. Based on the results of this study, the following conclusions are drawn:

- The hollow core concrete slab reinforced with GFRP bars behaved the same as the solid slab due to only a 9% reduction in the gross area of the concrete for hollow slab than the solid slab, and the area of concrete in compression for hollow slab was located above the hollow core. Slab S2 (hollow) showed a more brittle final failure than slab S1 (solid) because of the collapse of hollow core.
- The composite reinforcing system helped to enhance the structural performance of hollow core concrete slabs. The provision of three pieces of composite reinforcing

system (S3) increased the stiffness of the GFRP reinforced concrete hollow slab by 33%, reduced the loss of stiffness after concrete cracking by 24%, increased the load carrying capacity by 45%, and significantly increased the deformability by 117% than S2. The hollow composite system in slab S3 also prevented vertical flexural cracks starting from bottom and propagating up to the top layer of concrete, this resulted in ductile flexural failure.

- The hollow composite reinforcing system was more compatible with GFRP bars than steel bars due to their similar modulus of elasticity. The slab reinforced with steel (S4) was stiffer than S3 from the time the concrete began to crack until the steel yielded. However, the GFRP reinforced slab (S3) was stiffer and retained this constant stiffness until the load reached its maximum. Moreover, the GFRP bars and the CRS simultaneously resisted the load up to failure in S3, whereas all the load was transferred to CRS once the steel yielded in steel reinforced slab (S4).
- The simplified fibre model analysis reliably predicted the maximum flexural strength of hollow concrete slabs with composite reinforcing system. By incorporating the stiffening behaviour of concrete under tension and the flanges of the hollow composite reinforcing system, the predicted failure load was only 13.8% less than the failure load measured experimentally. This result was further verified with complex finite element analysis.

The above findings clearly demonstrated the effectiveness of CRS in concrete slabs. This enhancement in overall behaviour cannot be achieved with just conventional reinforcement or GFRP bars without the additional weight due to the increase in amount of reinforcement and the concrete itself. Moreover, a thinner concrete slab with CRS is possible to achieve more strength and stiffness than solid and hollow slab resulting in a more lightweight and efficient structural system. Thus, it is suggested that the effectiveness of CRS with different diameters

608 are explored in other types of structures to quantify further its benefit and to develop new light-
609 weight and high-strength concrete structures suitable for civil engineering construction.

610 **Acknowledgements**

611 The authors wish to acknowledge the support from the Australian Research Council through
612 the Discovery scheme (DP180102208). The authors would also like to thank Composite
613 Reinforcement Solutions Pty. Ltd. for providing the hollow composite reinforcing systems, as
614 well as the technical staff and postgraduate students at the Centre for Future Materials (CFM)
615 in the University of Southern Queensland for helping to prepare and testing specimens.

616 **References**

617 [1] Yardim Y, Waleed A, Jaafar MS, Laseima S. AAC-concrete light weight precast composite
618 floor slab. Construction and Building Materials. 2013;40:405-10.
619 [2] Taylor R, Maher D, Hayes B. Effect of the arrangement of reinforcement on the behaviour
620 of reinforced concrete slabs. Magazine of concrete research. 1966;18:85-94.
621 [3] Smith P. Design and specification of marine concrete structures. Marine Concrete Structures:
622 Design, Durability and Performance. 2016:65.
623 [4] Dalton N. Warning to check for 'concrete cancer' in older unit high rise complexes. Australia:
624 Cairns Post; 2014.
625 [5] Goldston MW. Behaviour of concrete beams reinforced with GFRP bars under static &
626 impact loading. Australia: University of Wollongong, 2016.
627 [6] Ferdous W, Ngo TD, Nguyen KTQ, Ghazlan A, Mendis P, Manalo A. Effect of fire-
628 retardant ceram powder on the properties of phenolic-based GFRP composites. Composites Part
629 B: Engineering. 2018;155:414-24.
630 [7] Abdalla H. Evaluation of deflection in concrete members reinforced with fibre reinforced
631 polymer (FRP) bars. Composite structures. 2002;56:63-71.
632 [8] Ferdous W, Manalo A, Aravinthan T. Effect of beam orientation on the static behaviour of
633 phenolic core sandwich composites with different shear span-to-depth ratios. Composite
634 Structures. 2017;168:292–304.
635 [9] Manalo AC. Behaviour of fibre composite sandwich structures under short and
636 asymmetrical beam shear tests. Composite Structures. 2013;99:339–49.
637 [10] Maranan G, Manalo A, Benmokrane B, Karunasena W, Mendis P. Evaluation of the
638 flexural strength and serviceability of geopolymer concrete beams reinforced with glass-fibre-
639 reinforced polymer (GFRP) bars. Engineering Structures. 2015;101:529-41.
640 [11] Maranan G, Manalo A, Benmokrane B, Karunasena W, Mendis P. Behavior of
641 concentrically loaded geopolymer-concrete circular columns reinforced longitudinally and
642 transversely with GFRP bars. Engineering Structures. 2016;117:422-36.
643 [12] Bouguerra K, Ahmed E, El-Gamal S, Benmokrane B. Testing of full-scale concrete bridge
644 deck slabs reinforced with fiber-reinforced polymer (FRP) bars. Construction and Building
645 Materials. 2011;25:3956-65.
646 [13] Sacks R, Eastman CM, Lee G. Parametric 3D modeling in building construction with
647 examples from precast concrete. Automation in construction. 2004;13:291-312.

[14] de Castilho VC, do Carmo Nicoletti M, El Debs MK. An investigation of the use of three selection-based genetic algorithm families when minimizing the production cost of hollow core slabs. Computer methods in applied mechanics and engineering. 2005;194:4651-67.
[15] Pajari M. Web shear failure in prestressed hollow core slabs. Journal of Structural Engineering. 2009;42:83-104.
[16] Hegger J, Roggendorf T, Kerkeni N. Shear capacity of prestressed hollow core slabs in slim floor constructions. Engineering Structures. 2009;31:551-9.
[17] Al-Negheimish AI, El-Sayed AK, Khanbari MO, Alhozaimy AM. Structural behavior of prestressed SCC hollow core slabs. Construction and Building Materials. 2018;182:334-45.
[18] Ferdous W, Bai Y, Ngo TD, Manalo A, Mendis P. New advancements, challenges and opportunities of multi-storey modular buildings – A state-of-the-art review. Engineering Structures. 2019;183:883-93.
[19] Azad AK, Hakeem IY. Flexural behavior of hybrid hollow-core slab built with ultra high performance concrete faces. Materials and Structures. 2016;49:3801-13.
[20] Brunesi E, Bolognini D, Nascimbene R. Evaluation of the shear capacity of precast-prestressed hollow core slabs: numerical and experimental comparisons. Materials and Structures. 2015;48:1503-21.
[21] Meng X. Shear Strengthening of Prestressed Hollow Core Slabs Using Externally Bonded Carbon Fiber Reinforced Polymer Sheets: University of Windsor (Canada), 2016.
[22] Cuenca E, Serna P. Failure modes and shear design of prestressed hollow core slabs made of fiber-reinforced concrete. Composites Part B: Engineering. 2013;45:952-64.
[23] Benayoune A, Samad AA, Trikha D, Ali AA, Ellinna S. Flexural behaviour of pre-cast concrete sandwich composite panel–experimental and theoretical investigations. Construction and Building Materials. 2008;22:580-92.
[24] Hall J, Mottram J. Combined FRP reinforcement and permanent formwork for concrete members. Journal of Composites for Construction. 1998;2:78-86.
[25] ASTM-D792. Standard test methods for density and specific gravity (relative density) of plastics by displacement. West Conshohocken, PA: ASTM International; 2013.
[26] ASTM-D2584. Standard test method for ignition loss of cured reinforced resins. West Conshohocken, PA: ASTM International; 2018.
[27] ASTM-E1356. Standard test method for assignment of the glass transition temperatures by differential scanning calorimetry. West Conshohocken, PA: ASTM International; 2014.
[28] ASTM-D695. Standard test method for compressive properties of rigid plastics. West Conshohocken, PA: ASTM International; 2015.
[29] ISO-14125. Fibre-reinforced plastic composites -- Determination of flexural properties. International Organization for Standardization; 1998.
[30] ASTM-D2344. Standard test method for short-beam strength of polymer matrix composite materials and their laminates. West Conshohocken, PA: ASTM International; 2016.
[31] ASTM-D4475. Standard test method for apparent horizontal shear strength of pultruded reinforced plastic rods by the short-beam method. West Conshohocken, PA: ASTM International; 2016.
[32] ASTM-D790. Standard test methods for flexural properties of unreinforced and reinforced plastics and electrical insulating materials. West Conshohocken, PA: ASTM International; 2017.
[33] CSA-S807. Specification for fibre-reinforced polymers. Canadian Standards Association; 2010.
[34] Benmokrane B, Manalo A, Bouhet J-C, Mohamed K, Robert M. Effects of Diameter on the Durability of Glass Fiber–Reinforced Polymer Bars Conditioned in Alkaline Solution. Journal of Composites for Construction. 2017;21:04017040.

[35] ASTM-D4476. Standard test method for flexural properties of fiber reinforced pultruded plastic rods. West Conshohocken, PA: ASTM International; 2014.
[36] ASTM-D7205. Standard test method for tensile properties of fiber reinforced polymer matrix composite bars. West Conshohocken, PA: ASTM International; 2016.
[37] ACI-440.6M. Specification for carbon and glass fiber-reinforced polymer bar materials for concrete reinforcement. USA: ACI; 2008.
[38] Standards Australia. Specification and supply of concrete. AS1379-2007 Australia SIA Global; 2007.
[39] Standards Australia. Methods of testing concrete Method 1: Sampling of concrete. AS 10121-2014 Australia: Standards Australia; 2014.
[40] CSA-S806. Design and construction of building structures with fibre-reinforced polymers. Canadian Standards Association; 2012.
[41] ANSYS-Inc. ANSYS mechanical APDL introductory tutorials. 15.0 ed. USA2013.
[42] AS-3600. Concrete structures. Sydney, Australia: Standards Australia; 2017.
[43] Nilson A, Darwin D, Dolan C. Design of Concrete Structures. Europe: McGraw-Hill Education, 2015.
[44] CNR-DT-203. Guide for the design and construction of concrete structures reinforced with fibre-reinforced polymer bars. Rome, Italy: National Research Council (CNR); 2006.
[45] ACI-318. Building code requirements for structural concrete (ACI 318-08) and commentary. USA: American Concrete Institute; 2008.
[46] S807-10 CC. Specification for fibre reinforced polymers. Rexdale, Ontario, Canada. 2010.
[47] Elgabbas F, El-Ghandour A, Abdelrahman A, El-Dieb A. Different CFRP strengthening techniques for prestressed hollow core concrete slabs: Experimental study and analytical investigation. Composite structures. 2010;92:401-11.
[48] El-Nemr A, Ahmed EA, El-Safty A, Benmokrane B. Evaluation of the flexural strength and serviceability of concrete beams reinforced with different types of GFRP bars. Engineering Structures. 2018;173:606-19.
[49] Ali AH, Afifi MZ, Abdulsalam B, Haggag H, El Hashimy A, El-Sayed T, et al. Performance Evaluation of One-Way Concrete Slabs Reinforced with New Developed GFRP Bars. Materials Sciences and Applications. 2015;6:420.
[50] Benmokrane B, Chaallal O, Masmoudi R. Glass fibre reinforced plastic (GFRP) rebars for concrete structures. Construction and Building Materials. 1995;9:353-64.
[51] El-Gamal S, AbdulRahman B, Benmokrane B. Deflection Behaviour of Concrete Beams Reinforced with Different Types of GFRP Bars. Advances in FRP Composites in Civil Engineering: Springer; 2011. p. 279-82.
[52] Kugkwan C, Daewon S. Behavior of one-way concrete slabs reinforced with GFRP bars. Journal of Asian Architecture and Building Engineering. 2012;11:351-8.
[53] Muttashar M, Manalo A, Karunasena W, Lokuge W. Flexural behaviour of multi-celled GFRP composite beams with concrete infill: Experiment and theoretical analysis. Composite Structures. 2017;159:21-33.
[54] Manalo A, Surendar S, Van Erp G, Benmokrane B. Flexural behavior of an FRP sandwich system with glass-fiber skins and a phenolic core at elevated in-service temperature. Composite Structures. 2016;152:96-105.
[55] Muttashar M, Manalo A, Karunasena W, Lokuge W. Influence of infill concrete strength on the flexural behaviour of pultruded GFRP square beams. Composite Structures. 2016;145:58-67.
[56] Wolanski AJ. Flexural behavior of reinforced and prestressed concrete beams using finite element analysis. USA: Marquette University, 2004.